A Rotating Azimuthally Distributed Auroral Current System on Saturn Revealed by the Cassini Spacecraft

R. L. Guo[1,2,3]*, Z. H. Yao[1]*, W. R. Dunn[4], B. Palmaerts[2], N. Sergis[5,6], D. Grodent[2], S. V. Badman[7], S. Y. Ye[8], Z. Y. Pu[9], D. G. Mitchell[10], B. Z. Zhang[11], N. Achilleos[12], A. J. Coates[4,12], Y. Wei[1], J. H. Waite[13], N. Krupp[14], M. K. Dougherty[15]

[1] Key Laboratory of Earth and Planetary Physics, Institute of Geology and Geophysics, Chinese Academy of Sciences, Beijing 100029, China

[2] Laboratory for Planetary and Atmospheric Physics, STAR institute, Université de Liège, Liège 4000, Belgium

[3] Laboratory of Optical Astronomy and Solar-Terrestrial Environment, Institute of Space Sciences, School of Space Science and Physics, Shandong University, Weihai, Shandong, China.

[4] Mullard Space Science Laboratory, University College London, Holmbury St Mary, Dorking RH5 6NT, UK

[5] Office of Space Research and Technology, Academy of Athens, Athens 106 79, Greece

[6] Institute of Astronomy, Astrophysics, Space Applications and Remote Sensing, National Observatory of Athens, Athens 118 10, Greece

[7] Department of Physics, Lancaster University, Lancaster LA1 4YB, UK

[8] Department of Earth and Space Sciences, Southern University of Science and Technology, Shenzhen 518055, China

[9] School of Earth and Space Sciences, Peking University, Beijing 100871, China

[10] Applied Physics Laboratory, Johns Hopkins University, Laurel, Maryland 20723, USA

[11] Department of Earth Sciences, University of Hong Kong, Hong Kong, China

[12] Department of Physics and Astronomy, Centre for Planetary Sciences at UCL/Birkbeck, University College London, London WC1E 6BT, UK

[13] Southwest Research Institute, San Antonio, TX 78238, United States

[14] Max-Planck-Institut für Sonnensystemforschung, Göttingen 37077, Germany

[15] Faculty of Natural Sciences, Department of Physics, Imperial College London, London SW7 2AZ, UK

* Corresponding authors: R. L. Guo (Ruilong.guo@uliege.be), Z. H. Yao (z.yao@ucl.ac.uk)

Abstract

Stunning aurorae are mainly produced when accelerated electrons travel along magnetic field lines to collide with the atmosphere. The motion of electrons often corresponds to the evolution of a magnetic field-aligned current (FAC) system. In the terrestrial magnetosphere, the current system is formed at the nightside sector, and thus produces an auroral bulge at night. Due to the different energy sources between Saturn and the Earth, it is expected that their auroral current systems are fundamentally different, although the specific auroral driver at Saturn is poorly understood. Using simultaneous measurements of the aurora, particles, magnetic fields, and energetic neutral atoms, we reveal that a chain of paired currents, each of which includes a downward and an upward current branch, is formed in Saturn's magnetosphere that generates separated auroral patches. These findings inform similar auroral current structures between the Earth and Saturn, while the difference is that Saturn's unique mass and energy sources lead to a rotational characteristic.

Keywords: Planetary magnetospheres (997), Saturn (1426), Aurorae (2192).

1. Introduction

The global magnetic field of a planet can fend off the solar wind particles to form a magnetosphere. Various dynamic processes in the magnetosphere can accelerate particles originating from the solar wind or the natural moons (i.e., volcanos and water vapor). The Earth's magnetosphere is mainly driven by solar wind activities. Saturn's magnetosphere is usually considered as a rotationally driven system, while it could be substantially modulated by solar wind activities. The rotationally driven processes stretch the magnetosphere to form a disc-like magnetic configuration, i.e., the magnetodisc. Beyond the magnetodisc, the solar wind shapes the magnetosphere to form a stretched magnetotail on the nightside. A number of observations at Earth have shown that many fundamental plasma processes like magnetic reconnection and dipolarization serve as the critical mechanisms in producing FAC wedge in the nightside magnetotail and powering the stunning auroral bulges in the ionosphere (Boström 1964; McPherron, Russell, & Aubry 1973; Liu et al. 2015). Similarly, in the traditional model for Saturn's and Jupiter's magnetospheres, the rotationally-driven magnetic reconnection only occurs in the nightside. The reconnection site is triggered in the pre-night sector and can extend to the dawn-side magnetopause (Vasyliunas 1983).

Several mysteries regarding Saturn's magnetospheric dynamics can occur at all local times. For example, quasi-periodic energetic electron pulsations are one of the important phenomena in Saturn's magnetosphere and are found at all local times (Mitchell et al. 2016; Palmaerts et al. 2016b; Bader et al. 2019b). The quasi-periodic pulsations correlate with auroral pulsations and auroral hiss, and the latter is an indication of FACs (Mitchell et al. 2016; Bader et al. 2019b). However, the precise explanation of this pulsation has not been found yet. A recent study used a realistic plasma/field model showing that the field line resonance's third and fourth harmonic modes correspond to the quasi-periodic 1-hour pulsations (Rusaitis et al. 2021). Besides, a rotating auroral spiral structure was suggested to be related to the recurrence of magnetic dipolarization (Palmaerts et al. 2020). Further, the existence of auroral patches or auroral beads at Saturn may imply localized dynamic processes like shear flow ballooning instability (Radioti et al. 2019). These studies suggest that the magnetospheric dynamics driving aurorae in the ionosphere are complex and cannot be explained simply with traditional theories, urging for an improved model for the global Saturnian auroral processes.

Recent studies of Saturn's magnetosphere revealed that magnetic reconnection can also take place in the dayside magnetodisc (Guo et al. 2018a), which was unexpected from the traditional model. Comparing to the traditional nightside reconnection, the length scales of the dayside magnetodisc reconnection are relatively small (Delamere et al. 2015; Guo et al. 2018b). A further study demonstrates that the multiple small-scale reconnection regions are discretely distributed at all local times and are rotating with Saturn's magnetosphere (Guo et al. 2019). Besides the reconnection sites, recurrent magnetospheric dipolarization was also uncovered at Saturn's dayside magnetosphere (Yao et al. 2018). The discoveries of dayside magnetodisc reconnection and dipolarization provide crucial implications for interpreting the dayside auroral emissions on giant planets, which were often attributed to processes taking place on the magnetopause (Radioti et al. 2013). The rotating feature of the reconnection sites (Guo et al. 2019) and the recurrent dipolarization (Yao et al. 2018) also indicate a new cycling model that can advance the understanding of rotating phenomena in Saturn's magnetosphere and ionosphere.

In this letter, using observational data from Cassini, phenomena in both Saturn's magnetosphere and ionosphere are physically connected. We show that FACs chain the accelerated particles near the magnetosphere equator and auroral emission. More importantly, those chains rotate and act on a larger area than expected in traditional knowledge, i.e., also at dayside.

2. Observational Results

2.1. Rotating main auroral patches (RMAPs) and their magnetospheric context

Energetic particles are one of the major products in a magnetospheric region disturbed by various instabilities where particles are energized, and the magnetic morphology is distorted. Collisions between the energetic particles and background cold atoms can produce energetic neutral atoms (ENA) that could directly be imaged by the ion and neutral camera (INCA) on the Magnetosphere Imaging Instrument (MIMI) onboard Cassini (Krimigis et al. 2004). Fig. 1a displays an image of the ENA in Saturn's active magnetosphere on July 15th, 2008. The resolution of the ENA image recorded by Cassini was insufficient to reveal the details of the active regions. The field of view (FOV) was also limited and could not cover ENA information from all local times. Fortunately, during this time, the Cassini Ultraviolet Imaging Spectrograph (UVIS) instrument (Esposito et al. 2004) provided contemporaneous auroral counterparts for these magnetospheric events. Fig. 1b-1d display three selected auroral images in the southern ionosphere. (The whole consecutive sequence of the auroral images is shown in Fig. A1 in the Appendix. The images are projected on a polar map and viewed from above the north pole. From this point of view, a west-to-east rotation corresponds to a counterclockwise motion.).

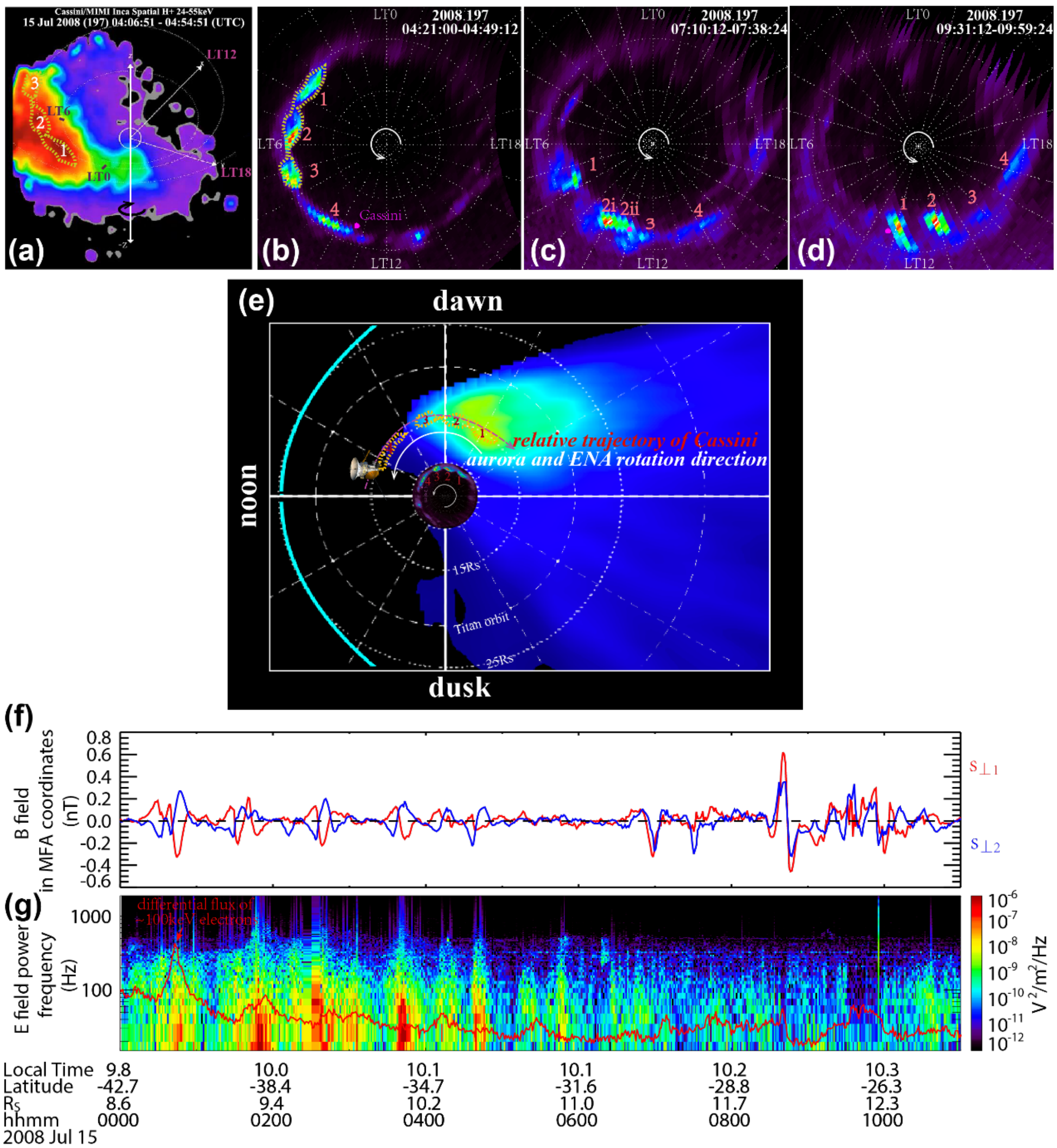

Figure 1. Connected phenomena due to the coupling processes between the ionosphere and magnetosphere. (**a**) 24–55 keV hydrogen ENA image recorded by the INCA instrument onboard Cassini from Saturn's southern hemisphere. (**b-d**) Images of the southern aurora from the Cassini-UVIS instrument and Cassini's magnetic footprint (magenta dot). The viewpoint is set above the north pole. So, the rotating direction is

anticlockwise for aurora but clockwise for ENA. The yellow dashed curve in **(b**) outlines patches ‘1’, ‘2’, and ‘3’, which is also simply mapped on the ENA image in (**a**) by considering only the corresponding Local Time but not the radial distance. (**e**) ENA images (the same time as shown in Fig. 1a) mapping on the equatorial plane while viewed from above the north pole. The Sun is on the left side of the plot. The two cyan curves represent the bow shock and magnetopause for presenting their relative positions to Saturn. The simultaneous aurora image (the same time as shown in Fig. 1b) is shown in the center of the plot. The yellow dashed curves accompanied with red numbers represent the auroral patches to show their local times (not mapping positions) relative to the ENA brightening area. The white curve with an arrow represents the rotation direction of the ENA, auroral patches, and the magnetosphere. The red dashed curve with an arrow represents the relative trajectory of Cassini due to the rotation of the magnetosphere. The auroral patches ‘1-3’ and the ENA brightening area collocated in the local time, while there is no ENA information for auroral patch ‘4’ due to the limitation of the field of view of the MIMI-INCA instrument. (**f**) Perturbations of the magnetic field recorded by the MAG instrument (Dougherty et al. 2004) in mean field-aligned (MFA) coordinates. The mean-field is determined by the low pass filtered data with a period of 20 min. The MFA coordinates applied in this paper are defined as follows: the **b** component (not shown) is parallel to the mean-field, $\mathbf{s}_{\perp 2}$ is perpendicular to the plane determined by the mean-field, and the line from Saturn to the spacecraft (opposite to corotation direction), and $\mathbf{s}_{\perp 1}$ completes the right-handed set. (**g**) Power spectrum of the electric field from the RPWS instrument (Gurnett et al. 2004). The red curve is the differential flux of the electrons from the C4 channel of the MIMI-LEMMS instrument (the same curve as the green one in Fig. 2d but scaled with a factor of 20 for co-plotting with the electric power spectrogram).

The successive auroral images in the Appendix show that a chain of auroral patches distribute in azimuth and rotate with Saturn and are named rotating main auroral patches (RMAPs) in this study. The RMAPs cover at least half of the main aurora region. The pink dots in the images mark the magnetic footprint of Cassini obtained by using the University College London/Achilleos-Guio-Arridge magnetodisc model (Achilleos, Guio, & Arridge 2010). The ionospheric latitude of the magnetic footprint of Cassini moves slowly from 73.7° to 72.9° during the ~6 hours of recording by UVIS. In addition to the mapping model, we used an Archimedean spiral equation to account for the bend-back effect of the magnetic field lines, as this substantially improves the local time (LT) mapping of Cassini’s position along the magnetic field lines into the ionosphere. The bend-back effect results in a deviation of $\Delta LT = 24(B_{\varphi}/B_r)\ln(\rho_{Cassini}/\rho_{Enceladus})/2\pi$ ranging from 0.3 to 0.8 hours between Cassini and its magnetic footprint, where $\rho_{Cassini}$ and $\rho_{Enceladus}$ are the perpendicular distances of Cassini and Enceladus from the spin axis of Saturn respectively.

Four distinct auroral patches at the dawn side polar region are labeled with numbers on the images. Previous literature has reported the spiral structure of auroral patch ‘1’ (Radioti et al. 2015). But the driving mechanism of the global auroral morphology, corresponding to the major energy dissipation processes in Saturn’s magnetosphere, is unknown. The averaged angular velocity can be calculated by tracing each auroral patch from image to image. We obtain a value of ~75% of rigid rotation (1 rotation per ~10.7 hours), similar to the value previously reported (Radioti et al. 2015). The ENA images in the equatorial plane also show corresponding rotating features, as seen in the full sequential records of the ENA images in Fig. A2 in the Appendix. (The ENA images are viewed from the actual location of Cassini, that is, from the southern hemisphere. From this point of view, a west-to-east rotation appears to move in the clockwise direction.) Although the detailed ENA structures cannot be clearly identified due to the limited temporal and spatial resolution of the INCA instrument, both the ENA and the aurora are consistently covering similar local times (see Fig. 1e and the yellow dashed outlines in Fig. 1a and 1b, bearing in mind the limitation of the FOVs for both INCA and UVIS instruments). Cassini was nearly motionless compared to the rotation of the magnetosphere. When seen in the frame rotating with the magnetosphere, Cassini swept over each of auroral patches (Cassini’s trajectory relative to the auroral patches is shown in Fig. 1e).

The Cassini magnetometer (MAG) instrument (Dougherty et al. 2004) detected a series of magnetic variations (Fig. 1f). The two curves in Fig. 1f are the $s_{\perp 1}$ and $s_{\perp 2}$ magnetic components in a mean field-aligned (MFA) coordinate system (detailed in the figure caption), in which the $s_{\perp 1}$ and $s_{\perp 2}$ directions are perpendicular to the mean magnetic field (averaged over 20 minutes) (Yao et al. 2017). The two perpendicular magnetic components suggest parallel currents flowing along the magnetic field lines, i.e., FACs. Fig. 1g shows the enhancements of the power spectrum density of the electric field detected by RPWS instrument (Gurnett et al. 2004). The enhanced waves represent auroral hiss and match the large magnetic perturbations, revealing a close relationship between the auroral hiss and FACs, as suggested in a previous study (Gurnett, Shawhan, & Shaw 1983). Besides, the differential flux of ~100keV electrons (red curve in Fig. 1g, from the C4 channel of the MIMI-LEMMS) recurrently enhances when recording the auroral hiss. Using simultaneous ENA measurements, UV auroral images, and auroral hiss signals, we can directly distinguish between spatial and temporal variations for these interconnected phenomena in this event, thereby putting forward a new global physical picture to explain all these observations. Here we provide direct evidence that the energetic electron recurrences associated with RMAPs observed for this interval are due to rotating spatial structures rather than temporal variations.

2.2. Multiple FAC system associated with RMAPs

Cassini flew through regions with evident magnetic field perturbations between 07:00 and 10:00 UT (Fig. 2a), which correspond to the FACs as indicated by the perpendicular magnetic perturbations in the MFA coordinates. The direction of FACs can be derived by applying the differential form of Ampere’s law to the observed magnetic field in Fig. 2a (detailed in the method section). The estimation is meaningful only when

Cassini is passing through the regions of FAC. During the interval plotted in Figure 2, Cassini was not in the magnetodisc, following the criteria of magnetodisc defined by Arridge et al. (2008) and described in the Appendix (See Fig. A3c). The latitude value of Cassini was lower than -26°, suggesting that Cassini was also far away from the cusp region. The region where Cassini stayed during the studied interval is the mid-latitude magnetosphere. Before the large magnetic perturbation, Cassini's MIMI-LEMMS instrument observed electron fluxes in Fig. 2e that peaked at an energy of ~100 eV before ~07:00 UT. When flying through the magnetic field perturbations, the energy of the peaking flux shows a sudden increase around 07:00 UT, and the fluxes of energetic electrons (Fig. 2d) are also notably enhanced. The large perturbations of both B_θ and B_φ magnetic components in Fig. 2a suggest Cassini flying through a disturbed magnetospheric region. The B_r magnetic component gradually varied from ~ -60 nT to ~ -14 nT, suggesting that the sudden electron flux enhancement was not caused by a rapid flapping of the current sheet. All the above pieces of evidence collectively indicate that, when recording the sudden change of hot electron flux, Cassini entered the FACs at mid-latitudes rather than other magnetospheric regions. The estimated FAC density $j_{//}'$ (see method) is represented by the area highlighted in blue/red in Fig. 2b, while blue indicating negative values (going out of the ionosphere) and red indicating positive values (going into the ionosphere).

The auroral intensity measured by UVIS at Cassini's magnetic footprint in the ionosphere is shown in Fig. 2c. The numbers for the intensity peaks indicate their corresponding auroral patches. The peaks of the auroral intensity generally coincide with the negative currents (electrons flowing into the ionosphere) (Fig. 2b) and the enhancements of the energetic electron flux (Fig. 2d). It should be noted that, due to the instrument geometry and limited FOV, the LEMMS instrument was unable to directly detect the electrons traveling along the magnetic field lines during this auroral event. Therefore, some enhancements of energetic electrons (e.g., the populations with velocities nearly perpendicular to the magnetic field lines) may not correspond to auroral emission. Nevertheless, the highly energetic (especially 100s keV) electrons indicate strong acceleration processes in the magnetosphere. The first auroral intensity peak corresponds to auroral patch '4'. Unfortunately, unlike patches '1-3', Cassini's footprint did not go through the center of the magnetospheric counterpart of auroral patch '4' (see Fig. A1a-A1c), so no recognizable heating is seen in the hot electron spectrum (Fig. 2e). A flux peak of the energetic electrons (Fig. 2d) (their large gyro-radii allow them to disperse into a large area at their source region) coincides with aurora patch '4' but was relatively weak compared to the signatures detected for patches '1-3'.

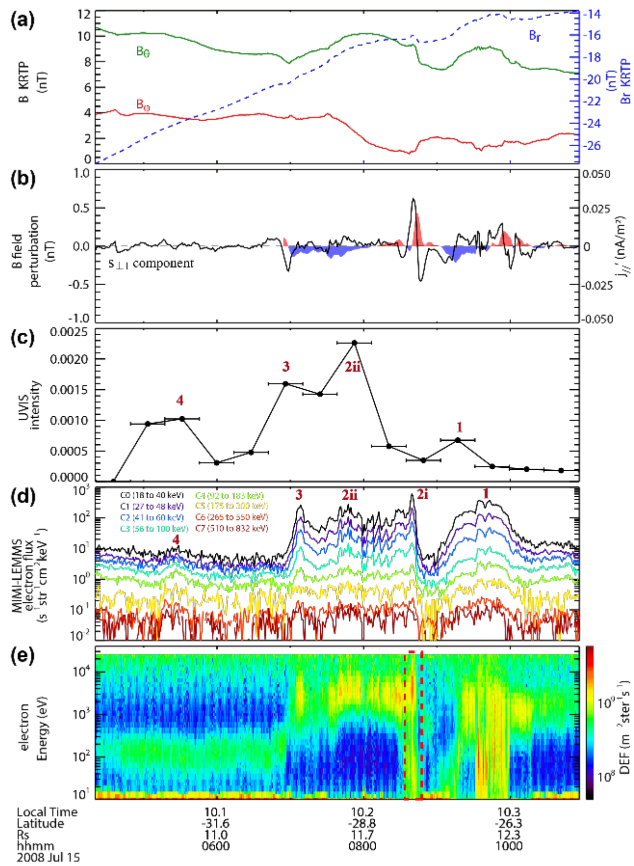

Figure 2. Relationship between FACs, auroral patches, and energetic electron enhancements. (**a**) B_θ (green), B_φ (red), and B_r (dashed blue) components of the magnetic field in the Kronographic Radial-Theta-Phi coordinates (KRTP, a spherical polar coordinate system). (**b**) The $\mathbf{s_{\perp 1}}$ component of the magnetic field (black curve). The area highlighted in blue/red show the estimated parallel current density $j_{//}'$: the blue indicating negative values (out of the ionosphere) and the red indicating positive values (going into the ionosphere). (**c**) Variation of the auroral intensity measured by UVIS instrument at the magnetic footprint of Cassini during the rotation of the aurorae (integrated over an area of 2°× 0.4 hours (Latitude × LT) that centered at Cassini's footprint). The horizontal segments show the integration time to obtain each aurora image. (**d**) Energetic electrons flux from the MIMI-LEMMS instrument. (**e**) Hot electron spectrum from the CAPS instrument (Young et al. 2004).

From 06:13 UT to 08:06 UT (see Fig. A1e-A1h in Appendix), the auroral morphology dynamically evolved: auroral patch '2' extended to momentarily merge with patch '3' and then separated again. The transient evolution of the active magnetospheric region related to aurora patch '2' resulted in two enhancements of the energetic electrons flux labeled '2ii' and '2i'. However, Cassini penetrated the FAC flowing into the ionosphere (positive parallel current in Fig. 2b) when recording electron enhancement '2i' (Fig. 2d) and matched a low UVIS intensity (Fig. 2c). The electrons with low energies around 100 eV enhanced at ‘2i’ in Fig. 2e show antiparallel pitch-angles (see Fig. A3d in Appendix), i.e., coming from the ionosphere, in agreement with the positive FAC current density. In summary, the energetic electron enhancements of ‘2ii’ and ‘2i’ are related to the FAC system of auroral patch ‘2’. As a consequence of the transient expansion of auroral patch ‘2’, the energetic electron flux during the interval from ‘3’ to ‘2i’ did not show a significant drop like the one shown in the interval between ‘2i’ to ‘1’.

The positive and negative currents appear alternatively, suggesting a chain of up-down current pairs associated with the RMAPs. This type of electrical current morphology often exists in the terrestrial auroral region and is characteristic of current wedgelets (Rostoker 1991; Forsyth et al. 2014; Liu et al. 2015), which are small scale structures compared to the major auroral intensifications, e.g., substorm auroral bulges. The energetic electrons do not show a discernible energy-time dispersion feature for each peak, indicating that the electrons were not transported from a remote region. The energetic electron flux was only enhanced when encountering the FACs that linked the isolated aurora beads, implying that the acceleration regions were separated in the magnetosphere.

Additionally, Table 1 gives a list of cases showing RMAPs and their contemporaneous recurrent energetic electrons and/or aurora hiss, demonstrating that the interconnections amongst ENA, multiple FAC, and main auroral patches are systematic in the Saturn system.

Table 1. List of patchy or beads-like aurora events.

IONOSPHERE	MID-LATITUDE MAGNETOSPHERE	EQUATOR
RMAPs events	**Corresponding Signatures in the duration including one period before and after RMAPs**	**Rotating ENA patch**
2008-197	SH, NDEE	yes
2008-238	SH, NDEE	yes
2016-229	SH	yes
2016-231	SH, NDEE	--
2016-275	SH	yes
2017-232	SH, NDEE	yes

SH: Separated Hiss as shown in Fig. 1g; **NDEE**: Non-Dispersion Energetic Electrons; **--**: no data

2.3. Recurrence of the Multiple FAC system

Fig. 3a and 3b show the comparison of the features in magnetic component B_φ perturbations and energetic electrons during the UVIS recording intervals (black curves) and the interval 11 hours later (red curves). These plots show a recurrence feature of the structures with a time scale of Saturn's rotation period, implying that the multiple FAC system can last longer than one planetary rotation period. The recurrence of the observational features may also be attributed to the rocking of the magnetosphere and the auroral oval (Bader et al. 2019a), which let Cassini penetrate the FACs during the intervals when the auroral oval was offset towards Cassini's footprint (Arridge et al. 2016). The difference between black and red curves may be attributed to the motion of Cassini (from ~ 12Rs to ~ 15Rs in distance to Saturn's center and from ~ -30° to ~ -15° in latitude) and/or the temporal evolution of the structures. For example, the transient evolution of auroral patch '2' produces a short-lived energetic electron flux peak before 08 UT (black curve in Fig. 3b), which disappears 11 hours later (red curve in Fig. 3b). Alongside the similarities between magnetic fields sampled from two planetary rotations (i.e., separated by about one planetary rotation), the energetic ions revealed by the ENA (Fig. A2 in Appendix) also recurred. This provides evidence that the active region may have lasted for more than one rotation period of Saturn and rotated at least once around Saturn to sweep past the spacecraft twice.

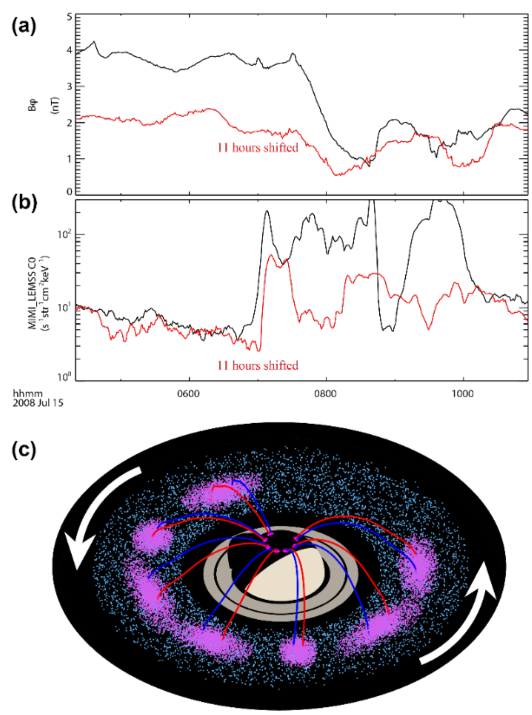

Figure 3. Recurrence of the magnetic structures and energetic electrons due to rotation. (**a-b**) B_ϕ component of magnetic field and electrons with an energy of 18-40 keV. The red curves are the 11-hours forward-shifted data. The difference between the shifted-time of 11 hours and the corotation period of 10.7 hours may be caused by the motion of Cassini from 10.2 hours to 10.5 hours in local time and the weakened bend-back effect during magnetospheric dynamics (Yao et al. 2018). (**c**) Sketch of the rotating

multiple FAC system and the patchy magnetospheric active regions (magenta areas in the equatorial plane can represent the ENA brightening areas). Cyan dots represent the magnetodisc. Magenta spots on the north polar region of Saturn (the hemispheroid at the center of the sketch) represent corresponding patchy aurorae. Blue and red curves represent FACs flowing into and out of the ionosphere, respectively. Although not shown in the sketch, symmetrical auroral patches and FACs can also be seen in Saturn's south pole.

3. Discussion and Summary

In this study, we report a rotating multiple FAC system in Saturn's magnetosphere. Although it shares a similar morphology with the terrestrial wedgelet current system (Forsyth et al. 2014), we notice that Saturn's multiple FAC systems are substantially different in both spatial and temporal scales. Fig. 3c illustrates the connection amongst the multiple FAC system, the ENA brightening areas, and the main auroral patches. Multiple active regions (magenta areas in the equatorial plane) link multiple auroral patches (magenta spots on the north polar region of Saturn) through complex FACs networks (Blue and red curves). The multiple FAC system may cover a larger area than Cassini detected, considering the limited FOV of both UVIS and INCA instruments. The auroral images and the recurrence of auroral hiss suggest that multiple FACs and active regions could be distributed discretely across much of the magnetosphere. Auroral hiss and the corresponding energetic electrons in Fig. 1g show that Cassini passed through several FACs before recording the UVIS images. The first aurora image in Fig. 1b also confirms that there are auroral patches duskward of Cassini's footprint, which probably have rotated from the dawn side a few hours ago.

The discovery of the multiple FAC system reported in this study provides a crucial constraint for theoretical investigations of the formation of Saturn's main auroral emission, which is probably also applicable to Jupiter. The recorded recurrence of energetic electrons is often associated with quasi-periodic electron pulsations. They were previously interpreted as temporal effects of the magnetospheric dynamics (Mitchell et al. 2009; Palmaerts et al. 2016a; Palmaerts et al. 2016b; Bader et al. 2019b), or the consequences of dynamical processes on magnetopause like Kelvin-Helmholtz waves (Masters et al. 2010), or magnetodisc reconnection occurring at dusk (Bader et al. 2019b). During RMAPs events, the slowly moving spacecraft would cross the relatively fast-rotating flux tubes connected to each auroral patch. Therefore, the rotation effect of the multiple active regions can lead to pulsating features in energetic electron data, e.g., the red curve in Fig. 1g. The planetary rotation induced 'electron pulsations' would complement previous physical interpretation on the commonly observed quasi-periodical phenomena.

During the rotation, the aurora is brighter on the dawn side than in the noon sector. The local time asymmetry in the auroral intensification may be explained by the fact that: (1) the formation of wedgelet currents is also accompanied by other processes that can contribute to auroral emissions, e.g., Alfvén waves. On the dawnside of the magnetosphere, the shear flow between the corotating magnetosphere and the tailward magnetosheath flow is maximum. Then, the Alfvénic Poynting flux associated with the wedgelets on the dawn side may be greater than at the other local times. (2) the wedgelets may experience a local time modulation (which is a common feature in giant planets' magnetosphere, e.g., (Carbary et al. 2017; Palmaerts et al. 2017)) during the rotation, causing asymmetric auroral intensification.

Although the wedgelet current system studied at Earth also contains multiple up-down FAC pairs and generates a chain of beads-like aurorae, it is limited to the nightside and cannot extend to the dayside. Its lifetime is on the order of a few minutes (Liang et al. 2008; Rae et al. 2009). The large spatial scale and long temporal scale of the multiple FACs on Saturn suggest that the mechanism for explaining the wedgelet current at Earth cannot be applied directly to Saturn's magnetosphere. The recent discoveries of dayside magnetodisc reconnection (Guo et al. 2018a) and dayside magnetic dipolarization (Yao et al. 2018) indicate that the dayside magnetic field lines could be more stretched than previously expected. When the field lines are stretched at all local times, fundamental plasma instabilities, like cross-field current instability, sausage instability, and ballooning/centrifugal instability (Lui 2004), may thus develop at any local time. Therefore, multiple FAC systems could be formed on a global scale. The multiple FAC system could also be a consequence of multiple long-standing small-scale reconnection sites distributed discretely in the magnetodisc (Guo et al. 2019). The multiple active regions existing at all local times can speed up the mass loss rate in Saturn's magnetosphere. It may be more critical at Jupiter, where internal processes predominantly drive magnetospheric dynamics.

Acknowledgments

Cassini operations are supported by NASA (managed by the Jet Propulsion Laboratory) and ESA. R.L.G thanks Japheth Yates and Aikaterini Radioti for their contribution to the discussions on the electron energizations and aurora emission. R.L.G. is supported by the Incoming Post-Docs in Sciences, Technology, Engineering, Materials and Agrobiotechnology (IPD-STEMA) project from Université de Liège. D.G. acknowledges the financial support from the Belgian Federal Science Policy Office (BELSPO) via the PRODEX Programme of ESA. B.P. is supported by the PRODEX program managed by ESA in collaboration with the Belgian Federal Science Policy Office. Z.Y. was supported by National Science Foundation of China (grant 42074211) and Key Research Program of the Institute of Geology & Geophysics CAS (grant IGGCAS-201904). S.V.B. was supported by UK STFC grants ST/V000748/1 and ST/M005534/1. A.J.C and W.R.D acknowledge support from UCL-MSSL solar system consolidated grant ST/S000240/1 from STFC, UK. The data from Cassini's MAG, CAPS, MIMI, RPWS, and UVIS instruments onboard the NASA/ESA Cassini spacecraft are available at https://pds-ppi.igpp.ucla.edu/.

APPENDIX

A. Estimation of the current density for the FAC

Since the angular velocity of the rotating magnetosphere is much larger than the speed of Cassini relative to Saturn, we may assume that Cassini remained fixed for the duration of an auroral event. Thus the motion of Cassini's foot-point relative to the planetary magnetic field was almost entirely due to the planetary rotation. In the spherical polar coordinates, as a preliminary estimation, we assume that r and θ of Cassini's position were constant while only φ was changing. We thus get $\delta\varphi = 2\pi C\delta t/P_{rigid}$, where $P_{rigid} \cong 10.7$ hours is the rigid rotation period of Saturn, and $C \approx 0.75$ is the ratio between the rotation speed of the aurora beads and the rigid rotation speed. The three components of the differential form of Ampere's law are:

$$\mu_0 j_r = {\partial B_\varphi}/{r\partial\theta} - {\partial B_\theta}/{r\sin\theta\,\partial\varphi};$$

$$\mu_0 j_\theta = {\partial B_r}/{r\sin\theta\,\partial\varphi} - {\partial B_\varphi}/{\partial r};$$

$$\mu_0 j_\varphi = {\partial B_\theta}/{\partial r} - {\partial B_r}/{r\partial\theta}.$$

In the case studied in this paper, we can calculate the terms with $\partial\varphi$: $j_r{}' = -\partial B_\theta/(\mu_0 r\sin\theta\,\partial\varphi)$ and $j_\theta{}' = \partial B_r/(\mu_0 r\sin\theta\,\partial\varphi)$. The combination of these two terms is the total variations in the φ direction caused by the current flow, i.e., independent of other directions. We can assume for simplicity that the FAC has a nearly circular transverse section, and the variation of the current density inside FAC during the concerned interval is not too big. For a columnar current structure, different directions of the current flow would cause opposite variation patterns along the φ direction. In other words, the combination of $j_r{}'$ and $j_\theta{}'$ can indicate the direction of the current flow.

Cassini was located in the southern magnetosphere and at the anti-planet-ward position (Sun-ward in this case) from the center of the FAC, as indicated by Cassini's magnetic footprint in the auroral images. At this position, in the FAC, increasing r and θ means moving in the direction from the FAC's center to the edge. According to the integral form of Ampere's law, the magnetic field generated by the FAC is stronger at the edge than that near the center. Hence, the increasing r and θ corresponds to an increase of $|B_\varphi|$. For the FAC parallel to the magnetic field, i.e., $j_{//} > 0$, the generated $B_{\varphi,FAC} < 0$, and $f = \partial B_\varphi/(\mu_0 r\partial\theta)$ and $g = \partial B_\varphi/(\mu_0\partial r)$ are negative. For the FAC antiparallel to the magnetic field, i.e., $j_{//} < 0$, the generated $B_{\varphi,FAC} > 0$, and both f and g are positive.

The direction of the averaged magnetic field line is $\boldsymbol{b_{averaged}} = [-0.66, 0.35, 0.09]$ in the Kronographic Radial-Theta-Phi coordinates coordinate when Cassini was inside FACs and did not change too much. Under the assumption that the current was parallel to the mean magnetic field line, j_φ is much smaller than the other two components and can be neglected in the estimation. The parallel current density $j_{//} = \boldsymbol{j}\cdot\boldsymbol{b_{averaged}} = -0.66j_r + 0.35j_\theta = -0.66j_r' + 0.35j_\theta' - (0.66f + 0.35g)$. Combining the above analysis, the term of $-(0.66f + 0.35g)$ has the same sign as $j_{//}$ in this case, i.e., the lack of f and g does not affect the sign of $j_{//}$. In Fig. 2b, we plot the $j_{//}{}' = b_r j_r{}' +$

$b_\theta j_\theta{}'$ by the color shaded areas to show the directions of the FACs. Since several assumptions are applied during the analysis, the current density amplitude is imprecise, and the error is hard to estimate. Even though, when the magnitude is large, the sign of $j_{//}{}'$ could be reliable to represent the sign of $j_{//}$, while the sign is what we really concern about in this study. The antiparallel low energy electrons in Fig. 2e and A3d are consistent with the positive FAC. Additionally, the sign of $j_{//}{}'$ is consistent with the bipolar signature of the $s_{\perp 1}$ magnetic component when crossing FAC transversely: the bipolar feature changing from positive to negative (from negative to positive) corresponds to positive (negative) $j_{//}$.

The estimation is valid under a quasi-steady state. The transient expansion of aurora patch '2' from 06:13 UT to 08:06 UT would bring relatively large uncertainty to the calculation and may also disturb the bipolar signature of the $s_{\perp 1}$magnetic component. Despite these, the existence of multiple FACs is explicit according to the measured magnetic perturbations.

The $s_{\perp 1}$ and $s_{\perp 2}$ components in the MFA coordinates only represent part of the FAC-induced magnetic variations. The 20-minute averaged magnetic field is not exactly the background field but contains part of the FAC-induced magnetic field. The total FAC-induced magnetic variation is on the order of several nTs, as shown in Fig. 2a. Despite this, the $s_{\perp 1}$ and $s_{\perp 2}$ components are helpful to demonstrate the finite structures of the FAC system.

B. Full sequential records of the auroral and ENA images

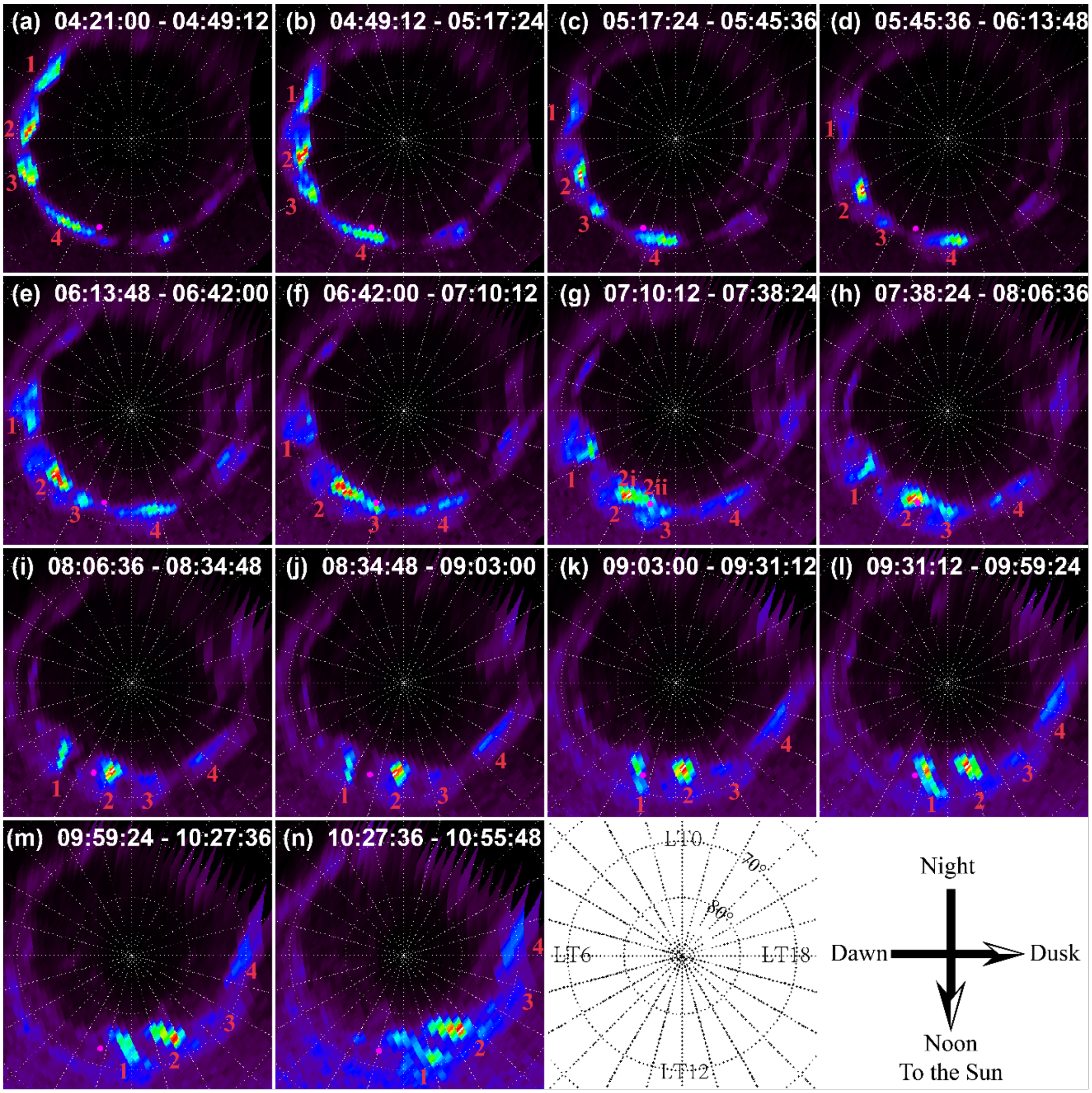

Fig. A1. Aurora images observed by UVIS instrument onboard Cassini. The aurorae were on the southern polar ionosphere, while the images were viewed above the north pole. The magenta dot in each image represents Cassini's magnetic footprint. A transient explosion of patch '2' starts at (**e**) and finishes at (**h**), which lasts about 1 hour.

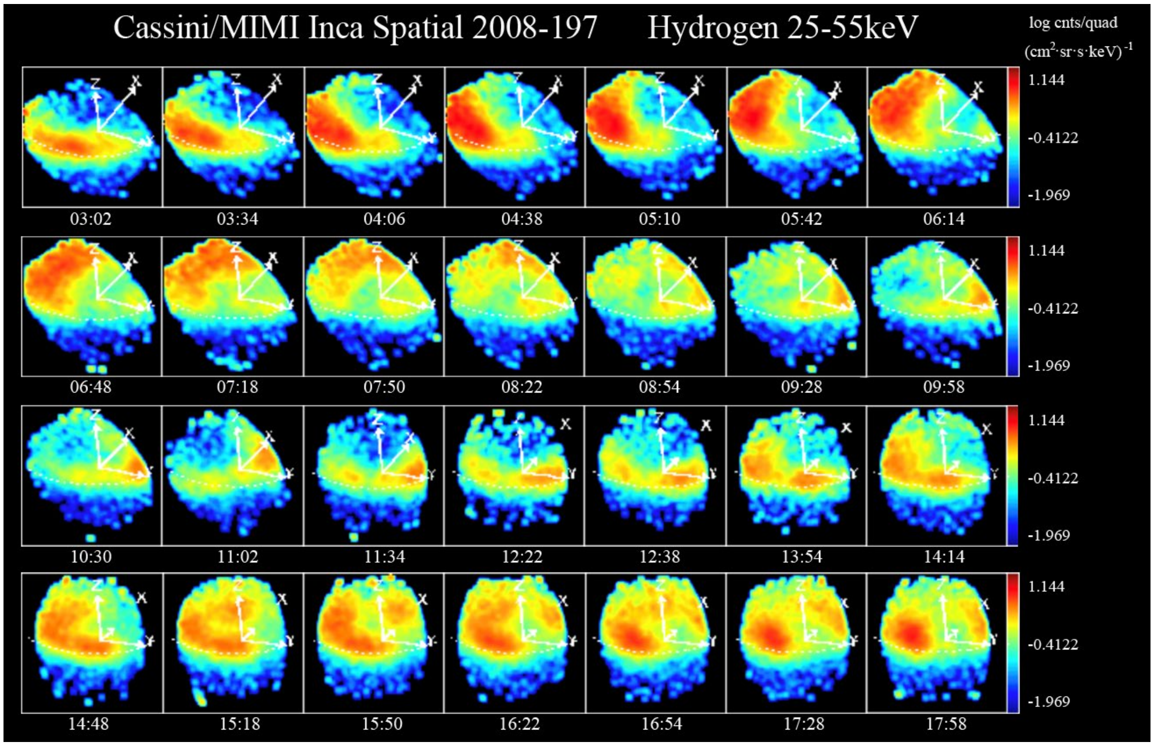

Fig. A2. ENA images on July 15th, 2008. Cassini was in the southern hemisphere when these images were taken. The time sequence shows the ENA rotated back after one rotation period.

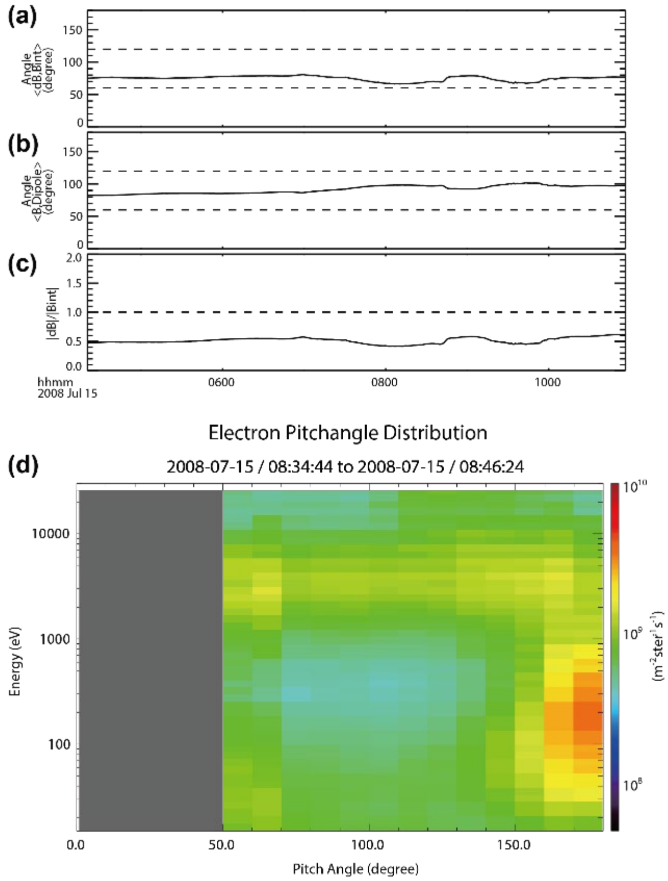

Fig. A3. (**a-c**) Criteria for classifying current-sheet-like magnetic field (Arridge et al. 2008). The two angles in (a) and (b) lie within 60 to 120 degrees, but in (c), the ratio between the magnetic deviation and the internal field is less than one. The deviation $|\mathbf{dB}| = |\mathbf{B}_{\mathbf{observation}} - \mathbf{B}_{\mathbf{internal}}|$, in where $\mathbf{B}_{\mathbf{observation}}$ is the observed magnetic field, and $\mathbf{B}_{\mathbf{internal}}$ is the internal magnetic field obtained from the Cassini 11 model (Dougherty et al. 2018). (**d**) The electron pitch angle-energy distribution generated during the interval is highlighted by the two red dashed vertical lines. The distributions indicate that the electrons with energies of ~100 eV are antiparallel, i.e., coming from the ionosphere. Note that we do not know parallel fluxes due to the instrumental limitation.

References

Achilleos, N., Guio, P., & Arridge, C. S. 2010, Monthly Notices of the Royal Astronomical Society, 401, 2349-2371

Arridge, C., Russell, C., Khurana, K., Achilleos, N., Cowley, S., Dougherty, M., Southwood, D., & Bunce, E. 2008, Journal of Geophysical Research: Space Physics, 113, A04214

Arridge, C. S., Jasinski, J. M., Achilleos, N., Bogdanova, Y. V., Bunce, E. J., Cowley, S. W. H., Fazakerley, A. N., Khurana, K. K., Lamy, L., Leisner, J. S., Roussos, E., Russell, C. T., Zarka, P., Coates, A. J., Dougherty, M. K., Jones, G. H., Krimigis, S. M., & Krupp, N. 2016, Journal of Geophysical Research: Space Physics, 121, 3006-3030

Bader, A., Badman, S. V., Kinrade, J., Cowley, S. W. H., Provan, G., & Pryor, W. 2019a, Journal of Geophysical Research: Space Physics, 124, 952-970

Bader, A., Badman, S. V., Yao, Z. H., Kinrade, J., & Pryor, W. R. 2019b, Journal of Geophysical Research: Space Physics, 124, 2451-2465

Boström, R. 1964, Journal of Geophysical Research, 69, 4983-4999

Carbary, J., F., Mitchell, D., G., Rymer, A., M., Krupp, N., Hamilton, D., Krimigis Stamatios, M., & Badman Sarah, V. 2017, Dawn ‐ Dusk Asymmetries in Planetary Plasma Environments, https://doi.org/10.1002/9781119216346.ch25

Delamere, P., Otto, A., Ma, X., Bagenal, F., & Wilson, R. 2015, Journal of Geophysical Research: Space Physics, 120, 4229-4245

Dougherty, M. K., Cao, H., Khurana, K. K., Hunt, G. J., Provan, G., Kellock, S., Burton, M. E., Burk, T. A., Bunce, E. J., Cowley, S. W. H., Kivelson, M. G., Russell, C. T., & Southwood, D. J. 2018, Science, 362

Dougherty, M. K., Kellock, S., Southwood, D. J., Balogh, A., Smith, E. J., Tsurutani, B. T., Gerlach, B., Glassmeier, K.-H., Gleim, F., Russell, C. T., Erdos, G., Neubauer, F. M., & Cowley, S. W. H. 2004, Space Science Reviews, 114, 331-383

Esposito, L. W., Barth, C. A., Colwell, J. E., Lawrence, G. M., McClintock, W. E., Stewart, A. I. F., Keller, H. U., Korth, A., Lauche, H., Festou, M. C., Lane, A. L., Hansen, C. J., Maki, J. N., West, R. A., Jahn, H., Reulke, R., Warlich, K., Shemansky, D. E., & Yung, Y. L. 2004, Space Science Reviews, 115, 299-361

Forsyth, C., Fazakerley, A. N., Rae, I. J., J. Watt, C. E., Murphy, K., Wild, J. A., Karlsson, T., Mutel, R., Owen, C. J., Ergun, R., Masson, A., Berthomier, M., Donovan, E., Frey, H. U., Matzka, J., Stolle, C., & Zhang, Y. 2014, Journal of Geophysical Research: Space Physics, 119, 927-946

Guo, R., Yao, Z., Wei, Y., Ray, L. C., Rae, I., Arridge, C. S., Coates, A., Delamere, P., Sergis, N., & Kollmann, P. 2018a, Nature Astronomy, 2, 640-645

Guo, R. L., Yao, Z. H., Sergis, N., Wei, Y., Mitchell, D., Roussos, E., Palmaerts, B., Dunn, W. R., Radioti, A., Ray, L. C., Coates, A. J., Grodent, D., Arridge, C. S., Kollmann, P., Krupp, N., Waite, J. H., Dougherty, M. K., Burch, J. L., & Wan, W. X. 2018b, The Astrophysical Journal Letters, 868, L23

Guo, R. L., Yao, Z. H., Sergis, N., Wei, Y., Xu, X. J., Coates, A. J., Delamere, P. A., Roussos, E., Arridge, C. S., Waite, J. H., Krupp, N., Mitchell, D., Burch, J., Dougherty, M. K., & Wan, W. X. 2019, The Astrophysical Journal, 884, L14

Gurnett, D. A., Kurth, W. S., Kirchner, D. L., Hospodarsky, G. B., Averkamp, T. F., Zarka, P., Lecacheux, A., Manning, R., Roux, A., Canu, P., Cornilleau-Wehrlin, N., Galopeau, P., Meyer, A., Boström, R., Gustafsson, G., Wahlund, J. E., Åhlen, L., Rucker, H. O., Ladreiter, H. P., Macher, W., Woolliscroft, L. J. C., Alleyne, H., Kaiser, M. L., Desch, M. D., Farrell, W. M., Harvey, C. C., Louarn, P., Kellogg, P. J., Goetz, K., & Pedersen, A. 2004, Space Science Reviews, 114, 395-463

Gurnett, D. A., Shawhan, S. D., & Shaw, R. R. 1983, Journal of Geophysical Research: Space Physics, 88, 329-340

Krimigis, S. M., Mitchell, D. G., Hamilton, D. C., Livi, S., Dandouras, J., Jaskulek, S., Armstrong, T. P., Boldt, J. D., Cheng, A. F., Gloeckler, G., Hayes, J. R., Hsieh, K. C., Ip, W.-H., Keath, E. P., Kirsch, E., Krupp, N., Lanzerotti, L. J., Lundgren, R., Mauk, B. H., McEntire, R. W., Roelof,

E. C., Schlemm, C. E., Tossman, B. E., Wilken, B., & Williams, D. J. 2004, Space Science Reviews, 114, 233-329

Liang, J., Donovan, E. F., Liu, W. W., Jackel, B., Syrjasuo, M., Mende, S. B., Frey, H. U., Angelopoulos, V., & Connors, M. 2008, Geophysical Research Letters, 35, L17S19

Liu, J., Angelopoulos, V., Chu, X., Zhou, X.-Z., & Yue, C. 2015, Geophysical Research Letters, 42, 1669-1676

Lui, A. T. Y. 2004, Space Science Reviews, 113, 127-206

Masters, A., Achilleos, N., Kivelson, M. G., Sergis, N., Dougherty, M. K., Thomsen, M. F., Arridge, C. S., Krimigis, S. M., McAndrews, H. J., Kanani, S. J., Krupp, N., & Coates, A. J. 2010, Journal of Geophysical Research: Space Physics, 115, A07225

McPherron, R. L., Russell, C. T., & Aubry, M. P. 1973, Journal of Geophysical Research (1896-1977), 78, 3131-3149

Mitchell, D., Krimigis, S., Paranicas, C., Brandt, P., Carbary, J., Roelof, E., Kurth, W., Gurnett, D., Clarke, J., & Nichols, J. 2009, Planetary and Space Science, 57, 1732-1742

Mitchell, D. G., Carbary, J. F., Bunce, E. J., Radioti, A., Badman, S. V., Pryor, W. R., Hospodarsky, G. B., & Kurth, W. S. 2016, Icarus, 263, 94-100

Palmaerts, B., Radioti, A., Roussos, E., Grodent, D., Gérard, J. C., Krupp, N., & Mitchell, D. G. 2016a, Journal of Geophysical Research: Space Physics, 121, 11,952-911,963

Palmaerts, B., Roussos, E., Krupp, N., Kurth, W. S., Mitchell, D. G., & Yates, J. N. 2016b, Icarus, 271, 1-18

Palmaerts, B., Vogt, M. F., Krupp, N., Grodent, D., & Bonfond, B. 2017, in Dawn‐Dusk Asymmetries in Planetary Plasma Environments, 307-322

Palmaerts, B., Yao, Z. H., Sergis, N., Guo, R. L., Grodent, D., Dialynas, K., Gerard, J. C., & Mitchell, D. G. 2020, Geophysical Research Letters, 47, e2020GL088810

Radioti, A., Grodent, D., Gérard, J. C., Bonfond, B., Gustin, J., Pryor, W., Jasinski, J., & Arridge, C. 2013, Geophysical Research Letters, 40, 4498-4502

Radioti, A., Grodent, D., Gérard, J. C., Roussos, E., Mitchell, D., Bonfond, B., & Pryor, W. 2015, Journal of Geophysical Research: Space Physics, 120, 8633-8643

Radioti, A., Yao, Z., Grodent, D., Palmaerts, B., Roussos, E., Dialynas, K., Mitchell, D., Pu, Z., Badman, S. V., Gérard, J. C., Pryor, W., & Bonfond, B. 2019, The Astrophysical Journal, 885, L16

Rae, I. J., Mann, I. R., Angelopoulos, V., Murphy, K. R., Milling, D. K., Kale, A., Frey, H. U., Rostoker, G., Russell, C. T., & Watt, C. E. 2009, Journal of Geophysical Research: Space Physics (1978–2012), 114

Rostoker, G. 1991, Magnetospheric Substorms, https://doi.org/10.1029/GM064p0061, 61-72

Rusaitis, L., Khurana, K. K., Kivelson, M. G., & Walker, R. J. 2021, Geophysical Research Letters, n/a, e2020GL090967

Vasyliunas, V. 1983, Physics of the Jovian magnetosphere, 1, 395-453

Yao, Z., Radioti, A., Rae, I., Liu, J., Grodent, D., Ray, L., Badman, S., Coates, A., Grard, J., Waite, J., Yates, J. N., Shi, Q. Q., Wei, Y., Bonfond, B., Dougherty, M., Roussos, E., Sergis, N., & Palmaerts, B. 2017, Geophysical Research Letters, 44, 11217-11228

Yao, Z. H., Radioti, A., Grodent, D., Ray, L. C., Palmaerts, B., Sergis, N., Dialynas, K., Coates, A. C., Arridge, C. S., Roussos, E., Badman, S. V., Ye, S.-Y., Gérard, J. C., Delamere, P. A., Guo, R. L., Pu, Z. Y., Waite, J. H., Krupp, N., Mitchell, D. G., & Dougherty, M. K. 2018, Journal of Geophysical Research: Space Physics, 123, 8502-8517

Young, D. T., Berthelier, J. J., Blanc, M., Burch, J. L., Coates, A. J., Goldstein, R., Grande, M., Hill, T. W., Johnson, R. E., Kelha, V., Mccomas, D. J., Sittler, E. C., Svenes, K. R., Szegö, K., Tanskanen, P., Ahola, K., Anderson, D., Bakshi, S., Baragiola, R. A., Barraclough, B. L., Black, R. K., Bolton, S., Booker, T., Bowman, R., Casey, P., Crary, F. J., Delapp, D., Dirks, G., Eaker, N., Funsten, H., Furman, J. D., Gosling, J. T., Hannula, H., Holmlund, C., Huomo, H., Illiano, J. M., Jensen, P., Johnson, M. A., Linder, D. R., Luntama, T., Maurice, S., Mccabe, K. P., Mursula, K., Narheim, B. T., Nordholt, J. E., Preece, A., Rudzki, J., Ruitberg, A., Smith, K., Szalai, S., Thomsen, M. F., Viherkanto, K., Vilppola, J., Vollmer, T., Wahl, T. E., Wüest, M., Ylikorpi, T., & Zinsmeyer, C. 2004, Space Science Reviews, 114, 1-112